Biosensors and Bioelectronics 168 (2020) 112554

Contents lists available at ScienceDirect

Biosensors and Bioelectronics

journal homepage: http://www.elsevier.com/locate/bios

Electrochemical biosensor for ultrasensitive exosomal miRNA analysis by cascade primer exchange reaction and MOF@Pt@MOF nanozyme

Xinyu Li [a,1], Xinmin Li [a,b,1], Dandan Li [c], Min Zhao [a], Haiping Wu [a], Bo Shen [b], Ping Liu [d], Shijia Ding [a,*]

[a] Key Laboratory of Clinical Laboratory Diagnostics (Ministry of Education), College of Laboratory Medicine, Chongqing Medical University, Chongqing, 400016, China
[b] Department of Laboratory Medicine, Chongqing Hospital of Traditional Chinese Medicine, Chongqing, 400016, China
[c] Department of Laboratory Medicine, The Second Affiliated Hospital of Chongqing Medical University, Chongqing, 400016, China
[d] Bioscience (Tianjin) Diagnostic Technology CO., LTD, Tianjin, 300000, China

ARTICLE INFO

Keywords:
Primer exchange reaction
Metal-organic frameworks
Nanozyme
Electrochemical biosensor
Exosomal miRNAs

ABSTRACT

Exosomal miRNAs have been discovered as important and reliable biomarkers for early diagnosis of tumors. However, it is still challenging to achieve accurate determination of trace exosomal miRNAs in real samples. Herein, we report an electrochemical strategy based on the cascade primer exchange reaction (PER) with MOF@Pt@MOF nanozyme for ultrasensitive detection of exosomal miRNA. Target-triggered PER that only includes a gated hairpin, a primer, and DNA polymerase can produce a long single strand in an autonomous and isothermal manner. Then, the nascent strand releases the protector B used to blockade capture probes, resulting in the binding of the nanozyme to sensing interface. Under the catalysis of the nanozyme, hydrogen peroxide (H_2O_2) is decomposed into H_2O and O_2, thus producing an amplified electrochemical signal. Benefiting from the cascade PER and the noticeable catalytic activity of the multiple-layered nanozyme, the established biosensor shows high sensitivity with limit of detection down to 0.29 fM and high specificity that can distinguish homologous miRNAs with single base mismatch. The developed strategy allows discrimination of tumor cells and breast cancer patients by detecting exosomal miRNA-21, and the results of this biosensor are consistent with qRT-PCR. Therefore, the electrochemical strategy has wide potential in the early screening of tumors.

1. Introduction

Exosomes are 40–160 nm saucer-like membrane vesicles and secreted by almost all cells (Kalluri and LeBleu, 2020; He et al., 2018). Studies have shown that exosomes are closely involved in various pathological processes through intercellular transfer of exosomal cargo molecules including nucleic acids, proteins, and liposomes (Skog et al., 2008; Ailawadi et al., 2015; Kulshreshtha et al., 2013). In particular, exosomal miRNAs (non-coding small molecule RNAs of around 22 nucleotides) can promote the development and progression of tumors by mediating the translation of messenger RNA (Tomasetti et al., 2017), such as ovarian, breast, and lung cancers (Thind and Wilson, 2016). Compared to miRNAs in peripheral blood, exosomal miRNAs exhibit high stability in the circulation due to the protection of exosomal membrane, and account for 76.20% of the total exosomal RNA (Hu et al., 2018; Cheng et al., 2014; Shao et al., 2018). Therefore, exosomal miRNAs have been regarded as reliable tumor biomarkers, which provide great diagnostic value in non-invasive detection of cancer (Mori et al., 2019; Sun et al., 2018). However, accurate detection of exosomal miRNAs remains a challenge owing to the low miRNAs abundance at early stages of tumors.

Currently, conventional quantitative reverse transcription polymerase chain reaction (qRT-PCR) is the dominating method for highly sensitive quantification of exosomal miRNAs (Tian et al., 2016). Nevertheless, the availability of qRT-PCR is substantially limited due to the demand of expensive experimental facilities, large laboratory scale, and complicated operation procedures. In this regard, a variety of methods have been developed for the detection of exosomal miRNAs, including molecular beacons (Zhang et al., 2017; Gao et al., 2019), nanoflares (Zhao et al., 2020; Wang et al., 2019a), rolling circle amplification (RCA) assisted CRISPR-Cas9 (Wang et al., 2020), and hybridization chain reaction etc (Wu et al., 2019; Guo et al., 2020).

* Corresponding author.
E-mail addresses: dingshijia@cqmu.edu.cn, dingshijia@163.com (S. Ding).
[1] X. Y. Li and X. M. Li contributed equally to this work.

https://doi.org/10.1016/j.bios.2020.112554
Received 14 July 2020; Received in revised form 19 August 2020; Accepted 23 August 2020
Available online 25 August 2020

Unfortunately, these reported methods usually require extra fluorescent tags, and reveal low sensitivity leading to the difficulty in detecting the low level of exosomal miRNAs. Hence, developing new sensing strategies with high specificity and sensitivity for detection of exosomal miRNAs remains urgent requirement.

Primer exchange reaction (PER) proposed by Yin's group is a robust signal amplification strategy, which has gained significant attention in the fields of biosensing and bioimaging (Kishi et al., 2018). In PER, a long single-stranded DNA with user-defined sequences is autonomously synthesized in an isothermal, programmable, and in site responsive pathway with the help of DNA polymerase. Unlike RCA that requires laborious synthesis of DNA circle and design of ligation strand, PER strategy can perform specific and rapid signal amplification only with a hairpin and a primer. Based on the PER, a series of high-performance biosensors have been explored for amplified and multiplexed imaging of protein, RNA, and DNA in cells and tissues (Kishi et al., 2019; Saka et al., 2019). Considering these superior characteristics, constructing a tailored PER strategy for detection of exosomal miRNA in real samples is highly desirable to further broaden its clinical application.

Nanozymes are one kind of nanomaterials with enzyme-mimicking catalytic properties, including platinum nanoparticles (Pt NPs), Fe_3O_4 NPs, and metal-organic frameworks (MOFs) (Wang et al., 2019b; Thompson and Cowan, 2020). Nanozymes are endowed with considerable advantages such as high stability, low cost, and good durability, which hold prodigious potential to serve as substitutes for traditional natural enzymes (Huang et al., 2019). In particular, MOF is favored by the researchers due to their excellent porosity, high surface area, and tailorable chemistry (Meng et al., 2020; Lu et al., 2018; Fang et al., 2020). Compared to individual MOF structure, MOF nanozymes coordinated other functional species with multi-layered features show obvious superiorities for catalytic activities, which have been explored for applications to sensing, catalysis, and tumor treatment (Li et al., 2019; Fu et al., 2019; Yang et al., 2020). For example, Pt NPs coated MOF (Ling et al., 2020), Au NPs encapsulated MOF (He et al., 2019), and MOF-on-MOF. (Lee et al., 2020; Ikigaki et al., 2019). Although these nanozymes enable enhanced properties, constructing multi-layered MOF-based nanozymes with higher catalytic activities still need many efforts.

Herein, we developed a novel electrochemical biosensor for exosomal miRNA-21 detection using target-triggered cascade PER with MOF@Pt@MOF nanozyme. In the presence of target, the nascent long DNA strand produced by the designed PER was used to expose capture probe for binding the nanozyme. The multi-layered nanozyme consisted of a layer of Pt NPs encapsulated between two layers of MIL-88, emerging an astonishing peroxidase-like activity toward H_2O_2 decomposition. By coating with single-stranded DNA (sDNA), the nanozyme could act as a signal probe (MIL-88@Pt@MIL-88@sDNA), producing amplified electrochemical signal. This biosensor features both the advantages of multiple-layered nanozyme and PER strategy for achieving trace exosomal miRNAs detection, which provides a robust sensing platform for early and accurate cancer diagnosis.

2. Experimental section

2.1. Materials and reagents

The oligonucleotides used in the biosensor (Table S1), qRT-PCR primers (Table S2), dATP, dTTP, and dCTP were purchased by Sangon Inc. (Shanghai, China). Klenow Fragment (KF) DNA polymerase was obtained from New England Biolabs Inc. (Beijing, China). N, N-dimethylformamide (DMF) was purchased from Kelong Chemical Inc. (Chengdu, China). Polyvinyl pyrrolidone (PVP), $H_2PtCl_6•6H_2O$, $FeCl_3•6H_2O$, 6-mercapto-1-hexanol (MCH), 2-aminoterephthalic acid (NH_2-BDC), H_2O_2, N-(3-dimethylaminopropyl)-N-ethylcarbodiimide hydrochloride (EDC), and N-hydroxysuccinimide (NHS), and horseradish peroxidase (HRP) were obtained from Sigma-Aldrich Chemical Co. (MO, USA). DL20 DNA marker was purchased from Takara (Dalian, China). Human breast cancer cell line (MCF-7) and non-tumorigenic epithelial cell line (MCF-10 A) were purchased from Procell (Wuhan, China). Dulbecco's modified eagle medium (DMEM) and fetal bovine serum (FBS) were purchased from Gibco (Shanghai, China). Universal microRNA purification kit was purchased from EZBioscience (Beijing, China). All-in-One™ miRNA qRT-PCR detection kit was bought from GeneCopoeia Inc. (Guangzhou, China). The serums of breast cancer patients and healthy persons were gained from the First Affiliated Hospital of Chongqing Medical University and approved by the medical ethics committee of the hospital. Deionized water (≥18 MΩ, Milli-Q, Millipore) was used in all experiments.

2.2. Apparatus

All electrochemical experiments were performed on a CHI660D electrochemical workstation (Shanghai Chenhua Instruments Co. Ltd., China) with a three-electrode system including a gold electrode (GE, working electrode), a platinum wire (counter electrode) and an Ag/AgCl electrode (reference electrode). The ultraviolet–visible (UV–vis) spectrophotometer (Shimadzu, Kyoto, Japan), transmission electron microscopy (TEM), and scanning electron microscope (SEM) (Hitachi, Tokyo, Japan) were applied to characterize the features and morphologies of nanomaterials. The electrophoresis apparatus (Bio-Rad Laboratories, Singapore) was chosen for the gel electrophoresis and the gel image was performed on the imaging system (Bio-Rad Laboratories, USA). qRT-PCR was performed and analyzed using CFX connect software (Bio-Rad, USA).

2.3. Synthesis of MIL-88

MIL-88 MOFs were synthesized according to the literature with some modification (Chen et al., 2016). Briefly, 0.126 g NH_2-BDC, 0.187 g $FeCl_3•6H_2O$, and 3.45 mmol acetic acid were dissolved in 15 mL DMF. Then the mixture was transferred to Teflon-liner and incubated at 120 °C for 4 h. After cooling to room temperature (RT), the particles were diluted with DMF and ethanol, followed by centrifugation at least 3 times (8000 rpm, 10 min) to fully remove the excess reactants. Finally, the obtained MIL-88 was resuspended in 8 mL DMF for further use.

2.4. Synthesis of MIL-88@Pt@MIL-88

Firstly, MIL-88@Pt was prepared according to the reported literature (Zhao et al., 2016). Briefly, 12 mL as-synthesized Pt NPs solution (synthesize details in Supplemental information) was added dropwise into 8 mL DMF of MIL-88 under vigorous stirring. After the mixed solution was stirred at RT for 2 h, MIL-88@Pt was collected by centrifugation at 8000 rpm for 10 min and washed twice with ethanol. Subsequently, the obtained MIL-88@Pt was resuspended in 12 mL DMF for synthesis of MIL-88@Pt@MIL-88 nanostructures. In a typical procedure, 12 mL DMF of MIL-88@Pt and 5 mL precursor solution (0.042 g NH_2-BDC and 0.062 g $FeCl_3•6H_2O$) were mixed, and then the mixed solution was heated at 120 °C for 8 h to grow MIL-88 shell onto the supported MIL-88@Pt. After that, the obtained product was collected by centrifugation at 5000 rpm for 10 min and washed twice with ethanol. Then, the obtained MIL-88@Pt@MIL-88 was dried at 80 °C overnight for later use.

2.5. Synthesis of signal probe

For signal probe (MIL-88@Pt@MIL-88@sDNA) fabrication, carboxylated sDNA (10 μM, 200 μL) was added to 500 μL of 400 mM EDC and 100 mM NHS, and reacted for 20 min at RT. Then, 200 μL MIL-88@Pt@MIL-88 aqueous solutions (1 mg mL^{-1}) were introduced into the above mixture and stirred at RT for 4 h. To remove the unconjugated sDNA and excessive EDC and NHS, the mixture was centrifuged (10,000 rpm, 10 min) and washed three times. Subsequently, the collected signal

probe was resuspended in 200 μL deionized water and stored at 4 °C for further use.

2.6. Electrochemical detection of exosomal miRNA-21

Cell culture, exosomes isolation and characterization, exosomal RNA isolation, qRT-PCR analysis, native polyacrylamide gel electrophoresis (PAGE), and modification of the GE surface were detailed in Supplemental information. To trigger the cascade PER, exosomal miRNA-21 with varied concentrations, 100 nM primers, and 10 nM gated hairpins were added into reaction solution (1 × ThermoPol buffer, 10 mM $MgCl_2$, 0.6 units/μL KF DNA polymerase, 0.1 mM dATP/dTTP/dCTP, 100 nM cleaner G). The cleaner G, cleanup hairpin, contained a template of C base which its 3' end could extend. The cleaner G was used to clean up a small amount of dGTP contamination in the reaction solution before the cascade PER. Then, the mixed solutions were incubated for 2 h and heated at 75 °C for 20 min to inactivate DNA polymerase. Subsequently, 10 μL PER products were dropped onto the modified GE for 100 min at 37 °C. Then, the GE was washed with PBS buffer (0.1 M, pH 7.4) to remove the unbounded substances. Further, 10 μL of signal probes was dropped onto the modified GE and incubated for 60 min at 37 °C. After the GE thoroughly washed with PBS buffer, the electrochemical assays were performed with differential pulse voltammetry (DPV) in N_2-saturated PBS buffer containing 2.0 mM H_2O_2. The potential was ranged from −0.4 to −1.0 V, pulse amplitudes of 0.07 V, pulse width of 0.05 s and sample width of 0.0167 s.

3. Results and discussion

3.1. Principle of the electrochemical biosensor

The electrochemical biosensor for exosomal miRNA-21 detection was developed based on the cascade PER and MOF@Pt@MOF nanozyme (Scheme 1). As illustrated in Scheme 1A, MIL-88@Pt@MIL-88 is stepwise synthesized by hydrothermal method and sequentially functionalized with carboxylated sDNA through the amidation reaction, forming MIL-88@Pt@MIL-88@sDNA nanocomposite that is used as electrochemical signal probe. As showed in Scheme 1B, the PER system only contains three components: primer, gated hairpin, and KF DNA polymerase. The gated hairpin consists of protector A and catalytic hairpin. The catalytic hairpin is designed a G-C pair as stop site to cease polymerization, due to the lack of dGTP in reaction buffer. Also, the catalytic hairpin and protector A are installed with an inverted dT on their 3′ end to prevent its non-specific extension. Added into the sensing system, exosomal miRNA-21 hybridizes with the protector A bound to the catalytic hairpin, forming miRNA-21@protector A double strand complex and transforming the gated hairpin into the catalytic hairpin. Subsequently, a primer specifically binds to the catalytic hairpin, which is extended by polymerase and halted at the stop site. Meanwhile, the extended sequence that is same with the primer dissociates from the catalytic hairpin once the copied sequence is competitively displaced by the domain on the hairpin. Then, the newly extended primer initiates the next extension cascade, thus growing autonomously a long DNA strand with tandem repetitive sequences. As depicted in Scheme 1C, the PER products hybridize and displace multiple protector B to unlock capture probes for binding signal probes. Finally, the signal probes tethered on sensing interface can effectively catalytic decomposition of H_2O_2, producing an obviously electrochemical signal for sensing exosomal miRNA-21.

3.2. Characterization of the multiple-layered MIL-88@Pt@MIL-88

To demonstrate the multiple-layered structure of MIL-88@Pt@MIL-88, the components of the nanomaterial were characterized step-by-step. As shown in Figs. S1A and B, TEM shows that the Pt NPs are largely monodispersed and roughly spherical. High-resolution TEM (HRTEM) indicates that each Pt NP is highly crystalline with the lattice spacing of 0.23 nm (Fig. S1C), corresponding to the (111) facet of face centered cubic Pt crystal (Borodko et al., 2012). The average particle diameter is found to be approximately 2.9 ± 0.4 nm (Fig. S1D), which is an optimal the size of Pt NPs according to these reported works (Tripković et al., 2014; Perez-Alonso et al., 2012). As shown in Fig. 1A and B, SEM and TEM results show that MIL-88 is characteristic of uniform octahedral morphology with the average size of about 200 nm. After decorating with Pt NPs, the Pt NPs are homogeneously dispersed on the surface of MIL-88 (Fig. 1C and D). After growing MIL-88 shell, the Pt NPs anchored at the MOF core seem to be covered and the size of obtained composites increase to about 250 nm (Fig. 1E and F), suggesting that the MOF@Pt@MOF complex is successfully synthesized. In addition, the thickness of MIL-88 shell is calculated to be 22.8 ± 3.2 nm

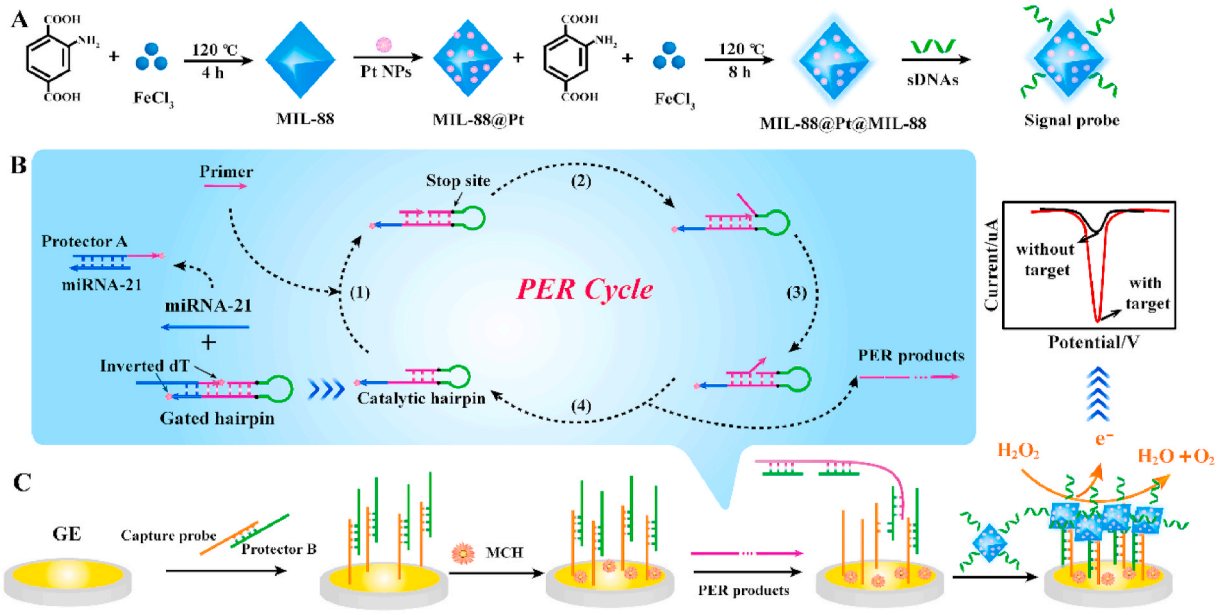

Scheme 1. Principle of the electrochemical biosensor based on the cascade PER and MOF@Pt@MOF nanozyme for the detection of exosomal miRNA-21. (A) The synthesis route of the MOF@Pt@MOF. (B) The operation mechanism of the cascade PER. (C) The electrochemical signal produced by MOF@Pt@MOF.

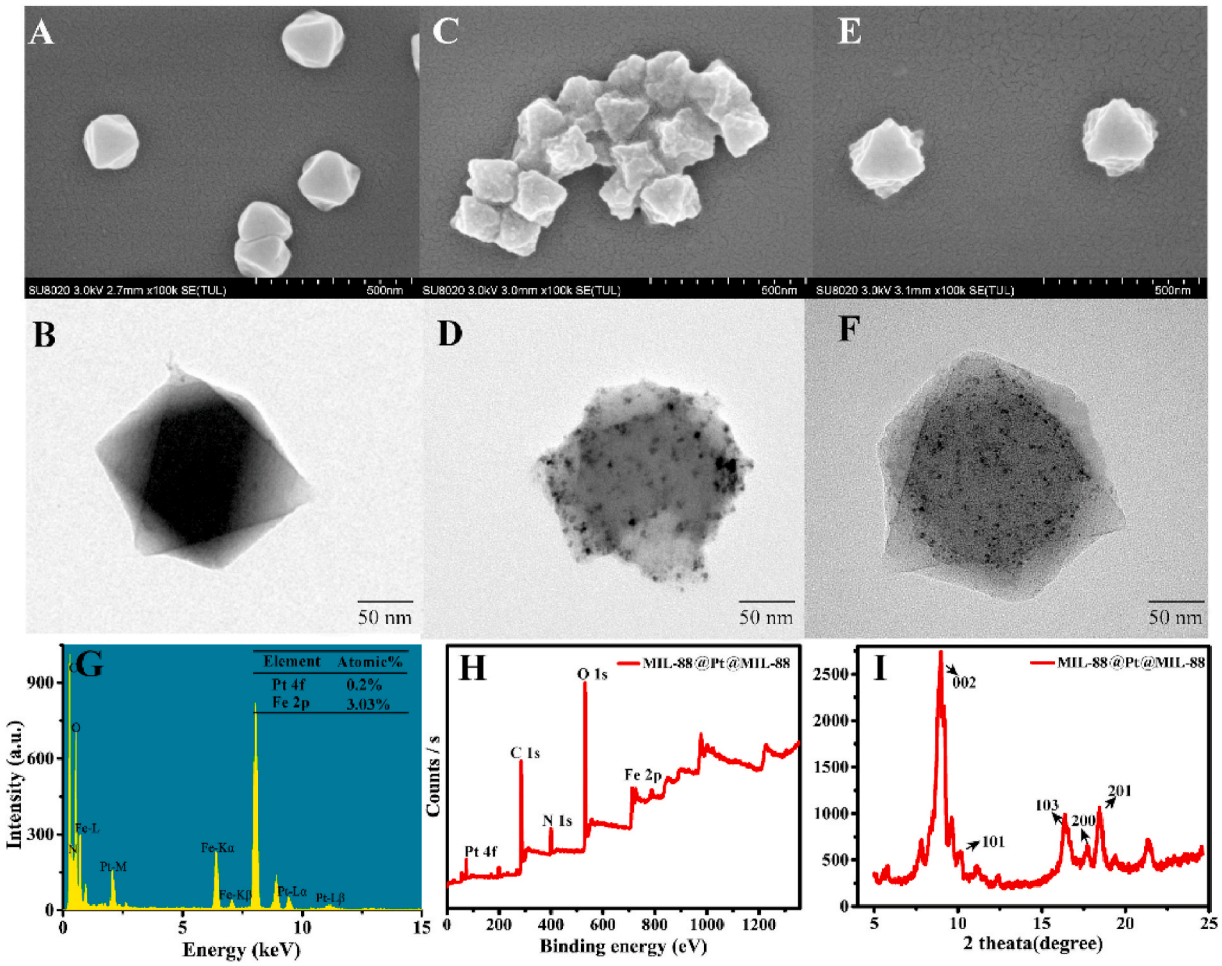

Fig. 1. SEM images of (A) MIL-88, (C) MIL-88@Pt, (E) MIL-88@Pt@MIL-88. TEM images of (B) MIL-88, (D) MIL-88@Pt, (F) MIL-88@Pt@MIL-88. (G) EDS image, (H) XPS spectra, and (I) XRD data of MIL-88@Pt@MIL-88.

based on the statistical results of TEM image (Fig. S2).

To confirm the chemical compositions of MIL-88@Pt@MIL-88, scanning TEM-energy dispersive spectroscopy (STEM-EDS), EDS, X-ray photoelectron spectroscopy (XPS), and X-ray diffraction (XRD) were performed. As shown in Fig. S3, STEM-EDS shows the Pt element are evenly distributed onto the entire Fe-MOF, indicating that the Pt NPs on the MIL-88 are synthesized successfully. As shown in Fig. 1G, the significant peaks for C, N, O, Fe and Pt are obtained in the EDS image, and the content of Pt NPs is 0.2% in the MIL-88@Pt@MIL-88. As shown in Fig. 1H, the characteristic peaks of Pt4f, C1s, N1s, O1s and Fe2p core level regions are obviously discovered in the XPS spectra. The XRD pattern of MIL-88@Pt@MIL88 with five diffraction peaks at 9.03, 11.5, 16.4, 17.8, and 18.6 indexes to the (002), (101), (103), (200), and (201) planes (Fig. 1I), which agrees with the typical XRD pattern of MIL-88 MOFs in the reference (Xie et al., 2015). The absence of XRD peaks from Pt nanocrystals could be probably attributed to the low NP concentration as well as the small size of encapsulated Pt NPs in the MIL-88 framework. These results further indicated the successful synthesis of MIL-88@Pt@MIL-88.

The porosity of the MOFs is a valuable advantage and it provides more sites for loading Pt NPs. By considering this, N_2 adsorption-desorption isotherms were performed to prove the adsorption capacity of MOFs. As shown in Fig. S4, the curve of MIL-88 displays type I, corresponding to the microporous material, and the curve of MIL-88@Pt composite exhibits a type IV hysteresis loop that is related to a mesoporous material. The Brunauer–Emmett–Teller (BET) surface area and micropore volume of MIL-88@Pt are calculated to be 76.9640 $m^2\ g^{-1}$ and 0.2606 $cm^3\ g^{-1}$, respectively, which is reduced compared to MIL-88 (101.5584 $m^2\ g^{-1}$ and 0.3530 $cm^3\ g^{-1}$). This is may be related to the occupation of the cavities of the MIL-88 framework by Pt NPs. The result is in good accordance with the previously published papers (Vu et al., 2017; Pooresmaeil and Namazi, 2020). In addition, the successful preparation of the MIL-88@Pt@MIL-88@sDNA was proved by UV–vis absorption spectra (Fig. S5).

3.3. Catalytic activity of MIL-88@Pt@MIL-88

To investigate the peroxidase-like activity of MIL-88@Pt@MIL-88, a typical catalytic oxidation reaction of the peroxidase substrate 3, 3′, 5, 5′-tetramethylbenzidine (TMB) by H_2O_2 was performed. The inset of Fig. 2A shows that different shades of blue solution are produced upon the addition of 5 μL of 1 mg mL^{-1} MIL-88 (a), MIL-88@Pt (b), and MIL-88@Pt@MIL-88 (c) to 500 μL the mixture of TMB and H_2O_2, respectively. Furthermore, these solutions were measured by UV–vis spectrophotometer. As shown in Fig. 2A, ignorable absorbance of oxidized TMB (oxTMB) at 650 nm is observed in the presence of MIL-88 (curve a), indicating the little catalytic activity of conventional MOF. When MIL-88@Pt are accessed, an improved absorbance of oxTMB are seen (curve b), suggesting that the combination of Pt NPs and MOF endows the MIL-88@Pt with enhanced catalytic activity. Surprisingly, a distinctly increased absorbance of oxTMB can be observed in the presence of MIL-88@Pt@MIL-88 (curve c). As shown in Fig. 2B, the absorbance slope of MIL-88@Pt@MIL-88 at 652 nm is nearly twice as big as MIL-88@Pt, four times higher than MIL-88, and slightly lower than HRP

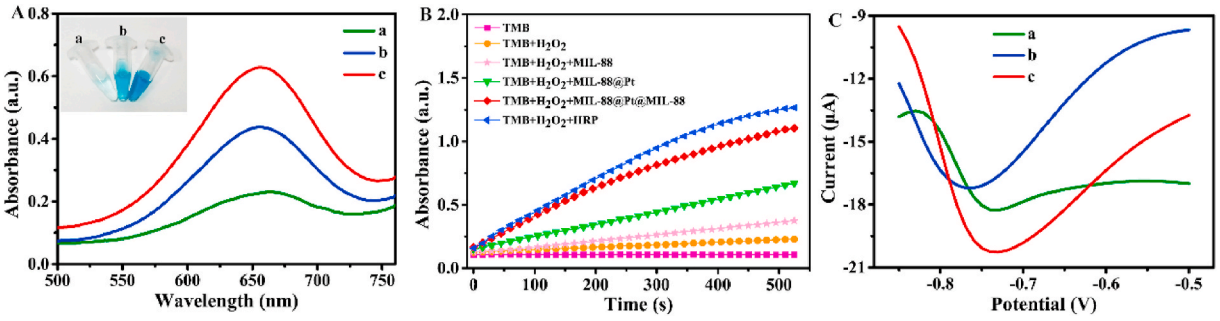

Fig. 2. Investigation of the catalytic activity of the nanozyme. (A) UV–vis absorption spectra of different reaction system: (a) H_2O_2 + TMB + MIL-88, (b) H_2O_2 + TMB + MIL-88@Pt, (c) H_2O_2 + TMB + MIL-88@Pt@MIL-88. (B) Time-dependent absorbance of oxTMB upon the addition of MIL-88, MIL-88@Pt, MIL-88@Pt@MIL-88, and HRP in TMB and H_2O_2 system. (C) The DPV response on catalyzing H_2O_2 of different reaction system: (a) MIL-88, (b) MIL-88@Pt, and (c) MIL-88@Pt@MIL-88.

in TMB and H_2O_2 system. These results demonstrated that the catalytic activity of MIL-88@Pt@MIL-88 was higher that MIL-88 and MIL-88@Pt and was comparable to HRP. In addition, the thickness of MIL-88 shell has little influence on the catalytic performance (Fig. S6).

Subsequently, the electrocatalytic activity of the nanozyme was also investigated. As shown in Fig. 2C, compared with the DPV signals of MIL-88 (curve a) and MIL-88@Pt (curve b), the MIL-88@Pt@MIL-88 (curve c) on catalyzing H_2O_2 exhibits the obvious increase of the reduction peak current. The results further demonstrated that the nanozyme of MIL-88@Pt@MIL-88 had more fascinating catalytic activity. The outstanding catalytic activity of the MIL-88@Pt@MIL-88 nanozyme might be attributed to its unique three-layered structure. The inner-layer MOF can provide larger surface area for anchoring numbers of Pt NPs. On the other hand, the outer-layer MOF can not only further stabilize the interlayer Pt NPs to mitigate aggregation, but also efficiently facilitate the mass transport during the catalytic reaction due to the porous nature.

3.4. Feasibility of the biosensor

To intuitive observe the operation process of the PER, PAGE experiment was firstly performed. As shown in Fig. 3A, lane 1, 2, 3 and 8 are corresponding to miRNA-21, protector A, catalytic hairpin and cleaner G, which only show a single band. The lanes of 4, 5, and 6 stand for miRNA-21@protector A, protector A@catalytic hairpin named as gated hairpin, and primer@catalytic hairpin complex, respectively. In the mixture of miRNA-21 and the gated hairpin, we can observe that miRNA-21 binds to protector A, forming miRNA-21@protector A complex, and the gated hairpin disappear (lane 7). As expected, miRNA-21 triggers the cascade PER, many ladder bands with larger mass (PER products) appear (lane 9). However, there are none of the miRNA-21 (lane 10) and primer (lane 11) in the system, the ladder bands are not seen, suggesting that the designed PER fails to operate. Then, electrochemical impedance spectroscopy and the cyclic voltammetry experiments were conducted to confirm the fabrication process of the biosensor (Fig. S7). To further evaluate the feasibility of the biosensor, DPV signals were recorded under different reaction conditions. As presented in Fig. 3B, a significantly enhanced DPV signal is observed in the presence of miRNA-21 compared to the blank control. Thus, these results clearly proved the feasibility of the proposed biosensor.

3.5. Analytical performance of the biosensor

To gain the optimal analytical performance, various reaction parameters of the electrochemical biosensor were optimized (Fig. S8). Under optimal experimental conditions, the sensitivity of the biosensor was investigated by varying miRNA-21 concentrations. Fig. 4A shows that the electrochemical signal increases with the increase of miRNA-21 concentrations from 1 fM to 1 nM. The correlation between the current signal change and the logarithm of miRNA-21 concentration displays a good linear relationship in the range of 1 fM to 1 nM (Fig. 4B). The fitted linear equation was $I = 1.63\lg C_{miRNA\text{-}21} + 13.71$ ($R^2 = 0.9962$), where I is the current intensity and C is the concentration of miRNA-21. The limit of detection (LOD) of 0.29 fM was evaluated based on a 3σb/slope, the σb stands for the standard deviation of three blank samples. In addition, the LOD of the electrochemical biosensor based on MIL-88@Pt was calculated to be 2.00 fM (Fig. S9), which was inferior compared to the electrochemical biosensor using MIL-88@Pt@MIL-88. Furthermore, contrasted with the methods previously reported for the detection of miRNAs in serums and exosomes, the biosensor showed superior sensitivity (Table S3). This is mainly attributed to the high electrocatalytic activity of the multiple-layered MIL-88@Pt@MIL-88 nanozyme and robust signal amplification ability of the tailored PER.

To evaluate the selectivity of the electrochemical biosensor, the

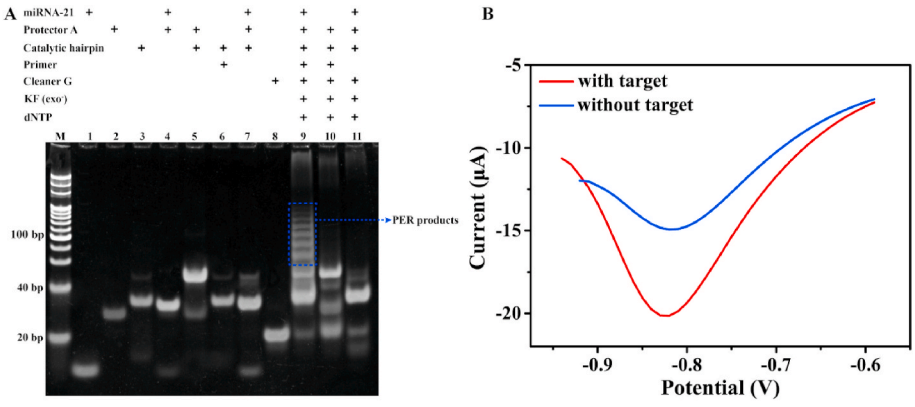

Fig. 3. Evaluation of the feasibility of the biosensor. (A) Verification of the reaction process of the designed PER by PAGE: (M) 20 bp DNA marker; (1) miRNA-21; (2) protector A; (3) catalytic hairpin; (4) miRNA-21 + protector A; (5) protector A + catalytic hairpin; (6) catalytic hairpin + primer; (7) miRNA-21 + protector A + catalytic hairpin; (8) cleaner G; (9) all components of the PER + miRNA-21; (10) all components of the PER; (11) all components of the PER except primer + miRNA-21. The concentrations of all DNA substrates of the PER except protector A are 1.0 μM. The concentrations of miRNA-21, KF polymerase, and protector A are 100 nM, 1.0 units/μL, and 1.2 μM, respectively. The incubation time is 2 h. (B) DPV signals responding to different reaction conditions. The concentration of target is 1 pM.

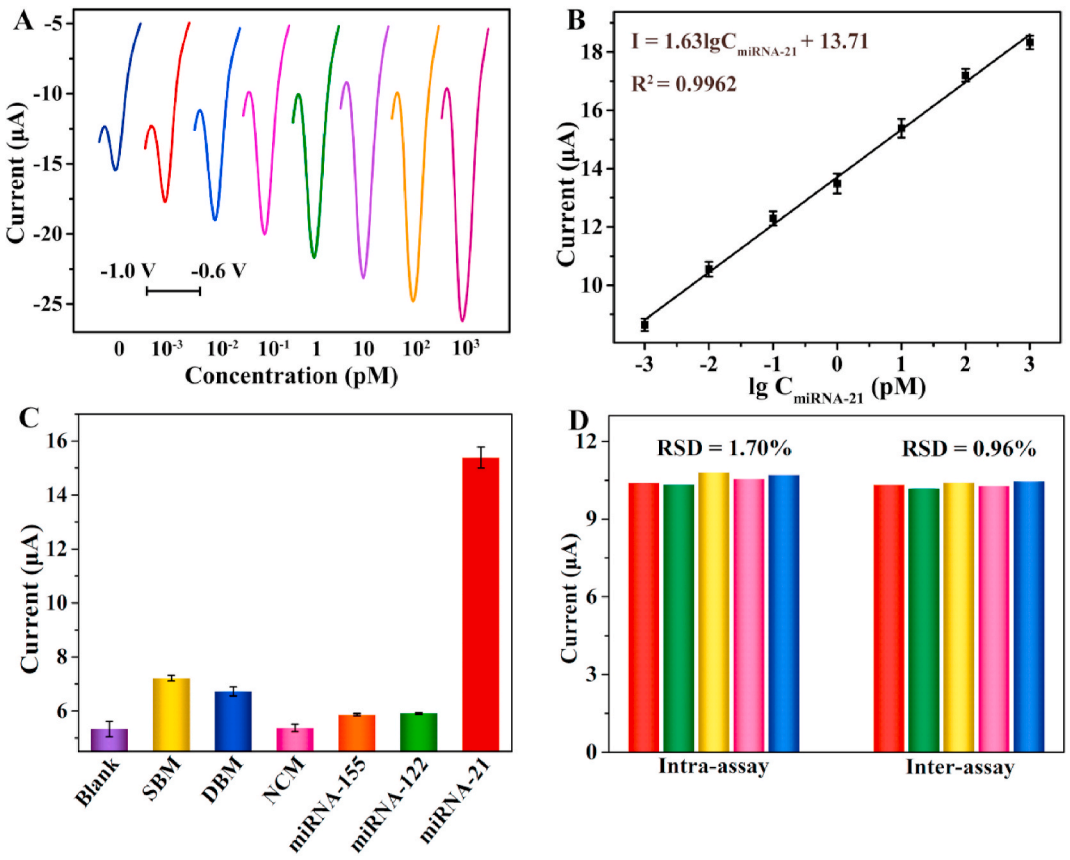

Fig. 4. Analytical performance of the electrochemical biosensor. (A) The DPV signals responding to miRNA-21 with different concentrations: 0, 10^{-3}, 10^{-2}, 10^{-1}, 1, 10, 10^{2} and 10^{3} pM. (B) The linear relationship of DPV signals versus $lgC_{miRNA-21}$. (C) Investigation of the specificity of the biosensor by comparing DPV signals responding to different miRNAs. The concentrations of SBM, DBM, NCM, miRNA-122, and miRNA-155 are 1 nM, respectively. The concentration of miRNA-21 is 10 pM. (D) Evaluation of the reproducibility of the biosensor by detecting 10 fM target. Data were expressed as mean ± standard deviations, sample replicates $n = 3$.

response signals produced by different similar miRNAs were compared. These miRNAs included single-base mismatch (SBM), double-base mismatch (DBM), non-complementary sequence (NCM), miRNA-122, and miRNA-155. As displayed in Fig. 4C, an obvious current change is observed in the presence of target (10 pM) compared to each interfering substance (1 nM). The results indicated the electrochemical biosensor was possessed of satisfactory selectivity. In addition, the reproducibility of the electrochemical biosensor was also evaluated by five individual measurements with 10 fM target. As shown in Fig. 4D, the relative standard deviation (RSD) value of intra- and inter-assays are as low as 1.70% and 0.96%, respectively, demonstrating that the biosensor has an excellent reproducibility.

3.6. Real samples analysis

To confirm whether the proposed biosensor could be applied in exosomal miRNAs detection in real samples, exosomal miRNA-21 derived from MCF-7 cells, MCF-10 A cells, and serums of breast cancer

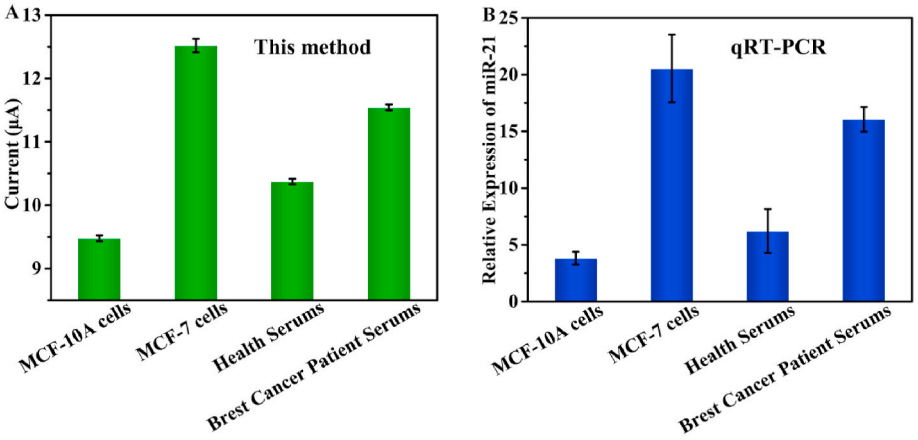

Fig. 5. Methodological comparison between the proposed biosensor and qRT-PCR. (A) The current intensity responding to exosomal miRNA-21 derived from four group samples. (B) The relative expression of exosomal miRNA-21 of determined by qRT-PCR. Data were expressed as mean ± standard deviations, sample replicates $n = 4$.

patient and health person were tested, respectively. As shown in Fig. 5A, the current intensities from MCF-7 cells and serum of breast cancer patient were higher than that from MCF-10 A cells and serum of health person. This result was consistent with the previous report that the expression level of miRNA-21 in breast cancer cell-derived exosomes was up-regulated (Wickramasinghe et al., 2009). To further verify the reliability of the developed electrochemical biosensor, the exosomal miRNA-21 derived from the four group samples was also analyzed by qRT-PCR. As shown in Fig. 5B, the detection results obtained by the qRT-PCR are the results of the developed biosensor. In addition, exosomal miRNA-122 was also detected by the developed biosensor (Fig. S10). These results demonstrated that the biosensor could serve as an alternative method for exosomal miRNAs detection, and held good potential in clinical applications.

4. Conclusion

In summary, an ultrasensitive electrochemical biosensor based on the cascade PER and multiple layered nanozyme has been developed for the detection of trace exosomal miRNA-21 in real samples. The synergistic effect between the tailored PER and multiple-layered nanozyme endows the developed biosensor with several considerable advantages. Firstly, target-triggered PER cascade can synthesize a long single-stranded DNA with simple sequence design in autonomous and homogeneous fashion. Secondly, owing to the characteristic nanostructure, inter-layer Pt NPs sandwiched between an inner-layer and an outer-layer MOF, the nanozyme exhibits extraordinary peroxidase-like catalytic performance. The three-layered nanozyme can not only produce obviously amplified electrochemical signal by decomposing H_2O_2, but also offers a new concept to synthesize other high-performance catalysts. More importantly, the biosensor possesses high sensitivity and specificity, and can be successfully applied in detecting exosomal miRNA-21 derived from real cells and peripheral blood samples. Therefore, the biosensor provides an alternative sensing platform for early diagnosis of cancer.

CRediT authorship contribution statement

Xinyu Li: Conceptualization, Methodology, Software, Investigation, Data curation, Writing - original draft, Project administration. **Xinmin Li:** Conceptualization, Methodology, Software, Investigation, Data curation, Writing - original draft, Project administration. **Dandan Li:** Software, Writing - original draft, Investigation. **Min Zhao:** Methodology, Formal analysis, Software. **Haiping Wu:** Methodology, Formal analysis, Software. **Bo Shen:** Conceptualization, Data curation. **Ping Liu:** Resources, Software, Validation. **Shijia Ding:** Supervision, Methodology, Data curation, Funding acquisition, Project administration, Data curation.

Declaration of competing interest

The authors declare that they have no known competing financial interests or personal relationships that could have appeared to influence the work reported in this paper.

Acknowledgements

This work was funded by the financial support from the National Natural Science Foundation of China (81873980, 81702083, 21804015), the National Science and Technology Major Project of the Ministry of Science and Technology of China (gs2%20:) (2018ZX10732202), the Natural Science Foundation Project of Chongqing (cstc2018jcyjAX0132), and the Xinglin Scholar Research Premotion Project of Chengdu University of TCM (YYZX20180029, YYZX20180030).

Appendix A. Supplementary data

Supplementary data to this article can be found online at https://doi.org/10.1016/j.bios.2020.112554.

References

Ailawadi, S., Wang, X., Gu, H., Fan, G., 2015. Biochim. Biophys. Acta 1852, 1–11.
Borodko, Y., Ercius, P., Pushkarev, V., Thompson, C., Somorjai, G.J., 2012. Phys. Chem. Lett. 3, 236–241.
Chen, J., Yu, C., Zhao, Y., Niu, Y., Zhang, L., Yu, Y., Wu, J., He, J., 2016. Biosens. Bioelectron. 91, 892–899.
Cheng, L., Sharples, R.A., Scicluna, B.J., Hill, A.F., 2014. J. Extracell. Vesicles 3, 23743.
Fang, R., Dhakshinamoorthy, A., Li, Y., Garcia, H., 2020. Chem. Soc. Rev. 49, 363–3687.
Fu, X., He, J., Zhang, C., Chen, J., Wen, Y., Li, J., Mao, W., Zhong, H., Wu, J., Ji, X., Yu, C., 2019. Biosens. Bioelectron. 132, 302–309.
Gao, X., Li, S., Ding, F., Fan, H., Shi, L., Zhu, L., Li, J., Feng, J., Zhu, X., Zhang, C., 2019. Angew. Chem., Int. Ed. Engl. 58, 8719–8723.
Guo, Q., Yu, Y., Zhang, H., Cai, C., Shen, Q., 2020. Anal. Chem. 92, 5302–5310.
He, C., Zheng, S., Luo, Y., Wang, B., 2018. Theranostics 8, 237–255.
He, Z., Huang, X., Wang, C., Li, X., Liu, Y., Zhou, Z., Wang, S., Zhang, F., Wang, Z., Jacobson, O., Zhu, J.J., Yu, G., Dai, Y., Chen, X., 2019. Angew. Chem. Int. Ed. Engl. 58, 8752–8756.
Hu, C., Chen, M., Jiang, R., Guo, Y., Wu, M., Zhang, X., 2018. J. Canc. 9, 3084–3092.
Huang, Y., Ren, J., Qu, X., 2019. Chem. Rev. 119, 4357–4412.
Ikigaki, K., Okada, K., Tokudome, Y., Toyao, T., Falcaro, P., Doonan, C.J., Takahashi, M., 2019. Angew. Chem. Int. Ed. Engl. 58, 6886–6890.
Kalluri, R., LeBleu, V.S., 2020. Science 367, eaau6977.
Kishi, J.Y., Lapan, S.W., Beliveau, B.J., West, E.R., Zhu, A., Sasaki, H.M., Saka, S.K., Wang, Y., Cepko, C.L., Yin, P., 2019. Nat. Methods 16, 533–544.
Kishi, J.Y., Schaus, T.E., Gopalkrishnan, N., Xuan, F., Yin, P., 2018. Nat. Chem. 10, 155–164.
Kulshreshtha, A., Ahmad, T., Agrawal, A., Ghosh, B., 2013. J. Allergy Clin. Immunol. 131, 1194–1203.
Lee, G., Lee, S., Oh, S., Kim, D., Oh, M., 2020. J. Am. Chem. Soc. 142, 3042–3049.
Li, B., Ma, J.G., Cheng, P., 2019. Small 15, e1804849.
Ling, P., Cheng, S., Chen, N., Qian, C., Gao, F., 2020. ACS Appl. Mater. Interfaces 12, 17185–17192.
Lu, K., Aung, T., Guo, N., Weichselbaum, R., Lin, W., 2018. Adv. Mater. 30, e1707634.
Meng, J., Liu, X., Niu, C., Pang, Q., Li, J., Liu, F., Liu, Z., Mai, L., 2020. Chem. Soc. Rev. 49, 3142–3186.
Mori, M.A., Ludwig, R.G., Garcia-Martin, R., Brandão, B.B., Kahn, C.R., 2019. Cell Metabol. 30, 656–673.
Perez-Alonso, F.J., Mccarthy, D.N., Nierhoff, A., Hernandez-Fernandez, P., Strebel, C., Stephens, I.E.L., 2012. Angew. Chem. Int. Ed. 51, 4641–4643.
Pooresmaeil, M., Namazi, H., 2020. Int. J. Biol. Macromol. 162, 501–511.
Saka, S.K., Wang, Y., Kishi, J.Y., Zhu, A., Zeng, Y., Xie, W., Kirli, K., Yapp, C., Cicconet, M., Beliveau, B.J., Lapan, S.W., Yin, S., Lin, M., Boyden, E.S., Kaeser, P.S., Pihan, G., Church, G.M., Yin, P., 2019. Nat. Biotechnol. 37, 1080–1090.
Shao, H., Im, H., Castro, C.M., Breakefield, X., Weissleder, R., Lee, H., 2018. Chem. Rev. 118, 1917–1950.
Skog, J., Würdinger, T., van Rijn, S., Meijer, D.H., Gainche, L., Curry, W.T., 2008. Nat. Cell Biol. 10, 1470–1476.
Sun, Z., Shi, K., Yang, S., Liu, J., Zhou, Q., Wang, G., Song, J., Li, Z., Zhang, Z., Yuan, W., 2018. Mol. Canc. 17, 147.
Thind, A., Wilson, C., 2016. J. Extracell. Vesicles 5, 31292.
Thompson, Z., Cowan, J.A., 2020. Small, e2000392.
Tian, H., Sun, Y., Liu, C., Duan, X., Tang, W., Li, Z., 2016. Anal. Chem. 88, 11384–11389.
Tomasetti, M., Lee, W., Santarelli, L., Neuzil, J., 2017. Exp. Mol. Med. 49, e285.
Tripković, V., Cerri, I., Bligaard, T., Rossmeisl, J., 2014. Catal. Lett. 144, 380–388.
Vu, T.A., Le, G.H., Vu, H.T., Nguyen, K.T., Quan, T.T.T., Nguyen, Q.K., 2017. Mater. Res. Express 4, 035038.
Wang, X., Yang, D., Liu, M., Cao, D., He, N., Wang, Z., 2019a. Biosens. Bioelectron. 137, 110–116.
Wang, H., Wan, K., Shi, X., 2019b. Adv. Mater. 31, e1805368.
Wang, R., Zhao, X., Chen, X., Qiu, X., Qing, G., Zhang, H., Zhang, L., Hu, X., He, Z., Zhong, D., Wang, Y., Luo, Y., 2020. Anal. Chem. 92, 2176–2185.
Wickramasinghe, N.S., Manavalan, T.T., Dougherty, S.M., Riggs, K.A., Li, Y., Klinge, C. M., 2009. Nucleic Acids Res. 37, 2584–2595.
Wu, Q., Wang, H., Gong, K., Shang, J., Liu, X., Wang, F., 2019. Anal. Chem. 91, 10172–10179.
Xie, S., Ye, J., Yuan, Y., Chai, Y., Yuan, R., 2015. Nanoscale 7, 18232–18238.
Yang, Y., Zhu, D., Liu, Y., Jiang, B., Jiang, W., Yan, X., Fan, K., 2020. Nanoscale 12, 13548–13557.
Zhang, J., Zhao, Q., Wu, Y., Zhang, B., Peng, W., Piao, J., Zhou, Y., Gao, W., Gong, X., Chang, J., 2017. Biosens. Bioelectron. 97, 26–33.
Zhao, J., Liu, C., Li, Y., Ma, Y., Deng, J., Li, L., Sun, J., 2020. J. Am. Chem. Soc. 142, 4996–5001.
Zhao, M., Yuan, K., Wang, Y., Li, G., Guo, J., Gu, L., 2016. Nature 539, 76–80.